


REPORT DOCUMENTATION PAGE					Form Approved OMB No. 0704-0188	
The public reporting burden for this collection of information is estimated to average 1 hour per response, including the time for reviewing instructions, searching existing data sources, gathering and maintaining the data needed, and completing and reviewing the collection of information. Send comments regarding this burden estimate or any other aspect of this collection of information, including suggestions for reducing the burden, to the Department of Defense, Executive Service and Communications Directorate (0704-0188). Respondents should be aware that notwithstanding any other provision of law, no person shall be subject to any penalty for failing to comply with a collection of information if it does not display a currently valid OMB control number.						
PLEASE DO NOT RETURN YOUR FORM TO THE ABOVE ORGANIZATION.						
1. REPORT DATE (DD-MM-YYYY) 10-06-2013		2. REPORT TYPE Book Chapter			3. DATES COVERED (From - To)	
4. TITLE AND SUBTITLE A Weak Constraint 4D-Var Assimilation System for the Navy Coastal Model Using the Representer Method				5a. CONTRACT NUMBER		
				5b. GRANT NUMBER		
				5c. PROGRAM ELEMENT NUMBER 0602435N		
				5d. PROJECT NUMBER		
6. AUTHOR(S) Hans Ngodock and Matthew Carrier				5e. TASK NUMBER		
				5f. WORK UNIT NUMBER 73-6531-02-5		
				5g. OTHER IDENTIFICATION NUMBER		
7. PERFORMING ORGANIZATION NAME(S) AND ADDRESS(ES) Naval Research Laboratory Oceanography Division Stennis Space Center, MS 39529-5004					8. PERFORMING ORGANIZATION REPORT NUMBER NRL/BC/7320-12-1052	
9. SPONSORING/MONITORING AGENCY NAME(S) AND ADDRESS(ES) Office of Naval Research One Liberty Center 875 North Randolph Street, Suite 1425 Arlington, VA 22203-1995					10. SPONSOR/MONITOR'S ACRONYM(S) ONR	
					11. SPONSOR/MONITOR'S REPORT NUMBER(S)	
12. DISTRIBUTION/AVAILABILITY STATEMENT Approved for public release, distribution is unlimited.						
20130613522						
13. SUPPLEMENTARY NOTES						
14. ABSTRACT A 4D-Variational system was recently developed for assimilating ocean observations with the Navy Coastal Ocean Model. It is described here, along with initial assimilation experiments in the Monterey Bay using a combination of real and synthetic ocean observations. For testing a new assimilation system it is advantageous to use this combination of real and synthetic data over simplified cases of climatology and twin data. Assimilation experiments are carried out in a weak constraint formulation, with the model's external forcing assumed to be erroneous in addition to initial conditions. The system's ability to fit assimilated and non assimilated observations is assessed, as well as the consistency and relevance of the retrieved model forcing. Experiment results show that the assimilation system fits the data with relatively high prior errors in the initial conditions and surface forcing fluxes. However, the retrieved model forcing errors are well within the range of acceptable corrections according to an independent study.						
15. SUBJECT TERMS variation data assimilation, representer methods, weak constraints, navy coastal ocean model, MODAS						
16. SECURITY CLASSIFICATION OF:			17. LIMITATION OF ABSTRACT UU	18. NUMBER OF PAGES 24	19a. NAME OF RESPONSIBLE PERSON Hans Ngodock	
a. REPORT Unclassified	b. ABSTRACT Unclassified	c. THIS PAGE Unclassified			19b. TELEPHONE NUMBER (Include area code) (228) 688-5455	

Seon Ki Park
Liang Xu *Editors*

Data Assimilation for Atmospheric, Oceanic and Hydrologic Applications (Vol. II)

 Springer

Chapter 15

A Weak Constraint 4D-Var Assimilation System for the Navy Coastal Ocean Model Using the Representer Method

Hans Ngodock and Matthew Carrier

Abstract A 4D-Variational system was recently developed for assimilating ocean observations with the Navy Coastal Ocean Model. It is described here, along with initial assimilation experiments in the Monterey Bay using a combination of real and synthetic ocean observations. For testing a new assimilation system it is advantageous to use this combination of real and synthetic data over simplified cases of climatology and twin data. Assimilation experiments are carried out in a weak constraint formulation, with the model's external forcing assumed to be erroneous in addition to initial conditions. The system's ability to fit assimilated and non assimilated observations is assessed, as well as the consistency and relevance of the retrieved model forcing. Experiment results show that the assimilation system fits the data with relatively high prior errors in the initial conditions and surface forcing fluxes. However, the retrieved model forcing errors are well within the range of acceptable corrections according to an independent study.

15.1 Introduction

This paper presents the development of a weak constraint 4D-Var data assimilation system based on the representer method (Bennett 1992, 2002) for the Navy Coastal Ocean Model (NCOM). NCOM is an operational ocean model that has been validated (Martin 2000; Barron et al. 2006). A major effort to implement state-of-the-art assimilation schemes was undertaken a few years ago, with the development of a 3DVAR, and a 4D-Var system based on the NCOM numerical code. The 3DVAR system is used for assimilation in global to regional scales, while the 4D-Var is to be used in limited area models with in-situ observations, provided initial and

H. Ngodock (✉) · M. Carrier

Naval Research Lab, code 7321, Stennis Space Center Hancock County, MS 39529, USA
e-mail: hans.ngodock@nrlssc.navy.mil

boundary conditions from a global or regional model assimilating with 3DVAR. Both the adjoint and linear perturbation (also called the forward representer) model codes were derived for the most part with the help of the Parametric Fortran compiler (PFC), Erwig et al. 2007.

Some general circulation models of the complexity of NCOM have seen similar efforts undertaken in the past decade: a 4D-Var assimilation system was developed for the Ocean Parallelisé (OPA) model (Weaver et al. 2003), for the MIT general circulation model (MITgcm, Marotzke et al. 1999) also used in the ECCO consortium assimilation experiments (Stammer et al. 2002), and a similar system was built for the regional ocean model system (ROMS), Moore et al. 2004. Unlike the other models using fixed z -levels (OPA and MITgcm) or s -coordinates (ROMS) NCOM uses a combination of both sigma layers, z -levels and a generalized vertical coordinate.

It is a common practice to test a recently developed assimilation system with climatological data or identical twin experiments in which the observations are simulated by the numerical model. There is hardly a case of failure in twin experiments, yet a successful assimilation with twin experiments never guarantees success with real data. On the other hand, climatological data are overly smooth in both space and time (due mostly to linear interpolation) and lack the variability associated with real observations. To avoid these simplified cases, the newly developed NCOM 4D-Var system is tested with real and synthetic observations generated by the modular ocean data assimilation system (MODAS) Fox et al. 2002, as well as with real observations collected from satellites and a fleet of gliders during the second autonomous ocean sampling network (AOSN II) in the Monterey Bay.

There are no specific applications of 4D-Var in the Monterey Bay, let alone its weak constraint formulation. Strong constraint variational assimilation (Broquet et al. 2009) has been applied to the California current system (CCS), including an application to estimate surface forcing correction (Broquet et al. 2011), using the inverse Regional Ocean Modeling System (IROMS, Di Lorenzo et al. 2007) with horizontal resolutions of 10 and 30 km. The CCS is a large area that includes the Monterey Bay, although these applications did not specifically target the Monterey Bay, given their rather coarse resolutions. Most of the assimilation experiments that have been carried for the Monterey Bay were based on sequential methods such as 3DVAR and ensemble-based Kalman filters: Chao et al. (2009), Haley et al. (2009), and Shulman et al. (2009). This study presents an application of the weak constraint 4D-Var in the Monterey Bay in a proof-of-concept context, using synthetic and real observations. The first objective is to demonstrate the system's ability to reduce large discrepancies between the model and the observations, when the latter are assigned very low errors. Therefore, this paper is more focused on the technical development of the weak constraint 4D-Var system.

A brief description of the numerical model is presented in the next section, followed by the 4D-Var system derivation and implementation in Sect. 15.3. Section 15.4 deals with the experiments setup and results, and concluding remarks follow in Sect. 15.5.

15.2 The Model

NCOM is described in the literature (Martin 2000; Barron et al. 2006). The description of the model equations given in the appendix is only repeated in order to exhibit the nonlinear terms in the model equations, as they directly affect the development of the linearized and adjoint models associated with NCOM. NCOM is a free surface model based on the primitive equations and employs the hydrostatic, Boussinesq and incompressible approximations. The model is discretized using finite differences on an Arakawa C-grid in the spatial dimensions. The equations are solved in three dimensions for momentum (both zonal and meridional components of velocity), temperature and salinity, and two dimensions for the free-surface mode: surface elevation and barotropic velocities.

The leapfrog scheme is used for time stepping in conjunction with an Asselin filter to avoid time splitting. All terms are treated explicitly in time except for the solution for the free surface and vertical diffusion. In the solution for the free surface, the surface pressure gradient terms in the depth-averaged momentum equations and the divergence terms in the depth-averaged continuity equation are evenly split between the old and new time levels to minimize the damping of surface waves. The model equations discretized with finite differences in flux-conservative form are given in the appendix.

The model domain used for this experiment contains the Monterey Bay, California region. This location is favorable for ocean modeling due to its strong land/sea breeze circulation patterns, complex coastline with steep topography, and the existence of frequent local upwelling and relaxation events (Shulman et al. 2002). The domain covers latitudes 35.6° – 37.49° North and longitudes 121.38° – 123.2° West with a horizontal resolution of 2 km and 41 layers in the vertical. The model was initialized on 01 August, 2003 and ran for one month to 01 September, 2003. The initial conditions were obtained from downscaling the operational $1/8^{\circ}$ resolution global NCOM to an intermediate model with horizontal resolution of 6 km, and then via a 3-to-1 nesting ratio to the 2 km model. Horizontal viscosities and diffusivities are computed using either the grid-cell Reynolds number (Re) or the Smagorinsky schemes, both of which tend to decrease as resolution is increased. The grid-cell Re scheme sets the mixing coefficient K to maintain a grid cell Re number below a specified value, e.g. if $Re = u * dx / K = 30$, then $K = u * dx / 30$. Hence, as dx decreases, K decreases proportionally. A similar computation is performed for the Smagorinsky scheme.

Surface boundary conditions (e.g. wind stress, IR radiation flux, etc.) are provided by the atmospheric mesoscale model COAMPS (Hodur 1997), which is run at the same horizontal resolution as the ocean model, with forcings archived every 12 h at the synoptic times of 0000 and 1200 UTC. Open boundary conditions use a combination of radiative models and prescribed values provided by the $1/8^{\circ}$ Global NCOM (GNCOM). Different radiative options are used at the open boundaries depending on the model state variables: a modified Orlanski radiative model is used for the tracer fields (temperature and salinity), an advective model for the zonal velocity (u), a zero gradient condition for the meridional velocity (v) as well as the barotropic velocities, and the Flather boundary condition for elevation.

15.3 The 4D-Var System

15.3.1 Linearization

Nonlinear terms in the model consist of all the advection terms in the momentum and tracer equations, the horizontal mixing with the Smagorinsky formula, the curvature correction, the vertical mixing with coefficients computed using the Mellor-Yamada 2.5 turbulence closure. Additional nonlinearities stem from the discretization in flux conservative form where vertical increments Δz in the sigma layers depend on the free surface elevation. As a consequence, even the time discretization is nonlinear. Nonlinearities also appear in the free surface, or barotropic mode, with the multiplication by the depth variables D^u and D^v in (15.23) and (15.24). However, the barotropic transports $D^u \bar{u}$ and $D^v \bar{v}$ are computed explicitly first, then the barotropic velocities (\bar{u} and \bar{v}) are derived by dividing the barotropic transports by the depth variable, which is a nonlinear operation. The baroclinic pressure gradient is computed from the density field obtained from the state equation as a nonlinear function of temperature and salinity. Other nonlinearities appear in the various radiative conditions at the open boundaries of the model domain mentioned above.

With the exception of the Mellor-Yamada turbulence closure, all of these nonlinear terms are linearized according to the first-order Taylor's approximation for the derivation of the tangent linear model.

For the sake of clarity, let's rewrite the leap-frog time discretization of (15.14), see the appendix, in the form

$$\frac{\Delta x^u \Delta y^u}{2\Delta t} \left((\Delta z^u)^{n+1} u^{n+1} - (\Delta z^u)^{n-1} u^{n-1} \right) = G^n, \quad (15.1)$$

where G^n represents the terms in the right hand side of (15.14) evaluated at time level n , and the depth increment $(\Delta z^u)^{n+1}$ is available from a previously computed elevation. The numerical model is updated by

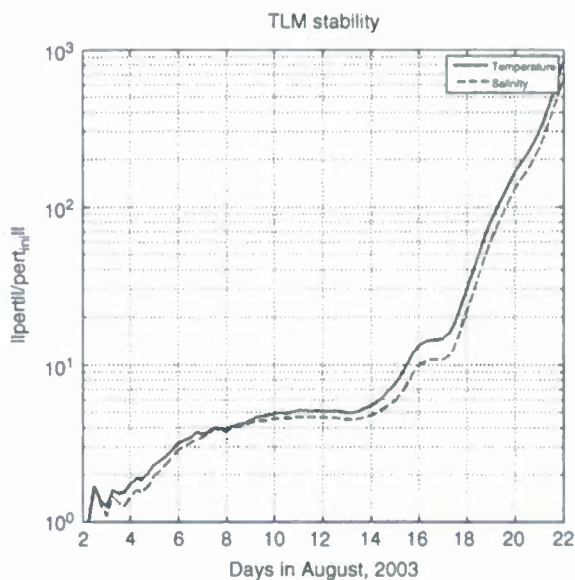
$$u^{n+1} = \frac{1}{(\Delta z^u)^{n+1}} \left[(\Delta z^u)^{n-1} u^{n-1} + \frac{2\Delta t}{\Delta x^u \Delta y^u} G^n \right] \quad (15.2)$$

The linearization of (15.2) is

$$\begin{aligned} \delta u^{n+1} = & \frac{1}{(\Delta z^u)^{n+1}} \left[(\Delta z^u)^{n-1} \delta u^{n-1} + (\delta \Delta z^u)^{n-1} u^{n-1} + \frac{2\Delta t}{\Delta x^u \Delta y^u} \delta G^n \right] \\ & - \frac{(\delta \Delta z^u)^{n+1}}{[(\Delta z^u)^{n+1}]^2} \left[(\Delta z^u)^{n-1} u^{n-1} + \frac{2\Delta t}{\Delta x^u \Delta y^u} G^n \right] \end{aligned} \quad (15.3)$$

where u is the background solution, i.e. the solution around which the model is linearized, G and Δz are computed using the background solution, and δu , δG and $\delta \Delta z$ are the linear perturbations of u , G and Δz respectively. In both (15.2)

Fig. 15.1 Time evolution of the magnitude of the perturbation to the temperature and salinity fields normalized by the magnitude of their respective initial perturbations



(and hence (15.3)) a small positive number is usually added to the denominator to prevent it from vanishing. As mentioned above the depth increments in the vertical discretization in NCOM depend on the time varying elevation only in the sigma layers. In the z-level portion of the vertical grid, (15.2) and (15.3) take the form

$$u^{n+1} = u^{n-1} + \frac{2\Delta t}{\Delta x^u \Delta y^u \Delta z^u} G^n \quad (15.4)$$

and

$$\delta u^{n+1} = \delta u^{n-1} + \frac{2\Delta t}{\Delta x^u \Delta y^u \Delta z^u} \delta G^n. \quad (15.5)$$

As for the vertical mixing coefficients from the Mellor-Yamada turbulence closure scheme, they are provided by the nonlinear model trajectory around which the model is linearized.

The stability of the linearized model is assessed by the time evolution of small perturbations: the tangent linear model is initialized by random three dimensional perturbations of the temperature and salinity fields and integrated over time. At each time step the norms of the perturbed temperature and salinity fields are computed and divided by the norms of their respective initial perturbations. Results plotted in Fig. 15.1 show that the linear perturbations are stable and bounded for about 12–15 days before they start to grow exponentially. Initial perturbations here are generated by the adjoint integration forced by Dirac impulses at randomly selected grid points. This process produces three-dimensional initial fields with dynamically coherent structures compared to purely random fields. However, the TLM test with purely random fields did not yield different results (not shown).

15.3.2 Adjoint Derivation

Once the linear perturbation model was obtained, the adjoint model was derived by transposition of the perturbation model as follows for both sigma layers and z-levels:

$$\begin{aligned}
 \lambda^* &= \lambda_u^{n+1} \\
 \lambda_u^{n+1} &= 0 \\
 \lambda_{\Delta z^u}^{n+1} &= \lambda_{\Delta z^u}^{n+1} - \frac{\lambda^*}{\left[(\Delta z^u)^{n+1}\right]^2} \left[(\Delta z^u)^{n-1} u^{n-1} + \frac{2\Delta t}{\Delta x^u \Delta y^u} G^n \right] \\
 \lambda_G^n &= \lambda_G^n + \frac{1}{(\Delta z^u)^{n+1}} \frac{2\Delta t}{\Delta x^u \Delta y^u} \lambda^* \\
 \lambda_{\Delta z^u}^{n-1} &= \lambda_{\Delta z^u}^{n-1} + \frac{u^{n-1}}{(\Delta z^u)^{n+1}} \lambda^* \\
 \lambda_u^{n-1} &= \lambda_u^{n-1} + \frac{(\Delta z^u)^{n-1}}{(\Delta z^u)^{n+1}} \lambda^*
 \end{aligned} \tag{15.6}$$

and

$$\begin{aligned}
 \lambda^* &= \lambda_u^{n+1} \\
 \lambda_u^{n+1} &= 0 \\
 \lambda_G^n &= \lambda_G^n + \frac{2\Delta t}{\Delta x^u \Delta y^u \Delta z^u} \lambda^* \\
 \lambda_u^{n-1} &= \lambda_u^{n-1} + \lambda^*
 \end{aligned} \tag{15.7}$$

where λ_a^i denotes the adjoint variable associated with the state variable a at the time level i , and λ^* is a temporary variable. In (15.6) and (15.7) it is assumed that the adjoint variables have been initialized at a prior time level. In practice, the model is usually computer programmed by subroutines, with individual terms of the model equations computed in separate subroutines. Similarly, the linearization and the adjoint derivation were carried out one subroutine at a time, and care was taken to ensure that symmetry between the linearized subroutine and its adjoint was preserved. The entire linearized model was obtained once every subroutine was linearized, and the entire adjoint was obtained with individual adjoint subroutines appearing in reverse order as compared to the linearized model.

In practice, both the linearized and adjoint models were obtained with the help of the Parametric Fortran compiler (PFC). Parametric Fortran is an extension of Fortran that supports defining Fortran program templates by allowing the parameterization

of arbitrary Fortran constructs. A Fortran program template can be translated into a regular Fortran program guided by values for the parameters. The Parametric Fortran compiler is written in Haskell (Peyton Jones 2003), and the parameter values are represented as Haskell values so they can be used by the Parametric Fortran compiler directly. Parametric Fortran is particularly useful in scientific computing. The applications include defining generic functions, removing duplicated code, and automatic differentiation. Parametric Fortran thus has broader and more general uses than previous tools in the likes of TAMC (Giering and Kaminski 1998), TAPENADE (Hascoet and Pascual 2004) or ADIFOR (Bischof et al. 1992), developed just for the purpose of automatic differentiation. The differentiation is based on the chain rule, with special treatment for non-differentiable functions.

15.3.3 *How PFC Works for TL and Adjoint Generation*

The Parametric Fortran compiler is publicly available from <http://web.engr.oregonstate.edu/~erwig/pf/>. It is a command line program in which the differentiation operation has been parameterized by "Diff". Assuming it has been installed on a user's computer, it can be used to generate tangent linear and adjoint of Fortran subroutines or programs in the following manner:

1. The user creates a parameter text file, say "param_file", in the format:
`Diff = TL [var1, var2, var3 ...]`
 where var1, var2, var3 ..., form a list of all active variables and all variables that depend or operate on active variables (including temporary variables), "TL" will indicate to the compiler that the tangent linear model is being created, and "Diff" is the differentiation parameter for Parametric Fortran.
2. For a subroutine "test.f" to be differentiated the user also creates a file "test.pf" that contains the subroutine in the form

```
{Diff:
Subroutine test(var1,var2...)
Body of subroutine
end
}
```
3. Finally, the compiler is invoked by typing the following from the command line: `pfc -p param_file test.pf test_TL.f`
 The output of the compiler will be the tangent linearized subroutine "test_TL.f".
4. The procedure for generating the adjoint is the same except that in steps 1 and 3 "TL" is replaced with "AD".

For generic state variables x and y and a subroutine computing a quantity Ax , the symmetry between the linearized subroutine and its adjoint is evaluated by

$$\langle Ax, y \rangle = \langle x, A^T y \rangle \quad (15.8)$$

where $\langle \cdot, \cdot \rangle$ denotes an inner product. This equality should hold to machine precision (regardless of computer architecture) not only for individual subroutines, but also for the entire linearized model and its adjoint. For randomly generated x and y as initial and final conditions for the linearized and adjoint models respectively, equality (15.8) was tested for integration periods of 1 and 5 days with an absolute difference in the order of 10^{-14} between the left and right hand side of (15.8), the computations being done in double precision.

Alternatively, this symmetry is also assessed by the symmetry of the representer matrix (Bennett 1992, 2002). For a given number M of observation locations (in the space-time domain), regardless of which model variable is observed, representer functions are computed, one per observation location. A representer function associated with a given observation location is obtained by integrating the adjoint model forced by a Dirac delta function centered at the chosen observation location, then using the adjoint solution (in space and time) as forcing for the perturbation model. A column of the representer matrix is computed by evaluating a representer function at all observation locations. If the adjoint model is consistently derived from the perturbation model, the representer matrix should be symmetric to the machine precision which is the case for our model and its adjoint.

15.3.4 The Cost Function

For sake of clarity, the model equations are rewritten in a simpler form

$$\begin{cases} \frac{\partial X}{\partial t} = F(X) + f, 0 \leq t \leq T \\ X(t=0) = I(x) + i(x) \end{cases} \quad (15.9)$$

where X stands for all the dependent model state variables: two dimensional sea surface height and barotropic velocities, and three dimensional temperature, salinity and baroclinic velocities, F is the model tendency terms in the right hand side of (15.14, 15.15, 15.16, 15.17 and 15.18) and (15.23, 15.24 and 15.25), f is the model error, a function of the independent variables (x and t) of the space-time domain Ω with covariance C_f , $I(x)$ is the prior initial condition, $i(x)$ is the initial condition error with covariance C_i . Given a vector Y of M observations of the model state in the space-time domain, with the associated vector of observation errors ε (with covariance C_ε),

$$y_m = H_m X + \varepsilon_m, \quad 1 \leq m \leq M \quad (15.10)$$

where H_m is the observation operator associated with the m th observation, one can define a weighted cost function

$$J = \int_0^T \int_{\Omega} \int_0^T \int_{\Omega} f(x, t) W_f(x, t, x', t') f(x', t') dx' dt' dx dt + \int_{\Omega} \int_{\Omega} i(x) W_i(x, x') i(x') dx' dx + \varepsilon^T W_{\varepsilon} \varepsilon \quad (15.11)$$

where Ω denotes the model domain, the weights W_f and W_i are defined as inverses of C_f and C_i in a convolution sense, and W_{ε} is the matrix inverse of C_{ε} . The latter is usually considered a diagonal matrix, from the assumption that observation errors are uncorrelated. Boundary condition errors are omitted from (15.9) to (15.11) only for the sake of clarity. The model error covariance is assumed to take the form

$$C_f(x, t, x', t') = \mathbf{v}(x)^{1/2} \mathbf{v}(x')^{1/2} \exp\left(-\frac{|x - x'|^2}{2L^2}\right) \exp\left(-\frac{|t - t'|}{\tau}\right) \quad (15.12)$$

where $\mathbf{v}(x)$ is the error variance and L and τ are the length and time scales respectively. The initial error covariance C_i assumes the form of (15.12) with the exception of the time correlation term and different (higher) variance. Horizontal correlations in (15.12) are obtained by solving a diffusion equation (Derber and Rosati 1989; Egbert et al. 1994; Weaver and Courtier 2001), while the time correlation is obtained by solving a pair of coupled Langevin equations (Chua and Bennett 2001; Bennett 2002; Ngodock 2005). Correlations in (15.12) are univariate and are implemented layer by layer for each model state variable. The cross correlations are provided by the model dynamics through the integration of the adjoint and the tangent linear models. Note that although the cost function is written with the inverse of the covariance functions, the actual inverses are not needed in practice, when the solution of the Euler-Lagrange equations associated with the minimization of (15.11) is sought through the representer method (Bennett 1992, 2002).

15.3.5 Error Standard Deviations: $\mathbf{v}(x)^{1/2}$

Assigning model errors and prescribing their covariances is the most difficult task in data assimilation, as acknowledged by most assimilation experts: Daley (1992), Talagrand (1999), Bennett (2002), Wunsch (2006). Not only are there many error sources (external forcing, initial and boundary conditions, bad parameterization, empirical formulation, unresolved processes), but also the errors cannot be measured. Therefore one can only make assumptions about them. Since NCOM includes

all resolvable processes and sub-gridscale parameterization, errors are attributed to the initial conditions and external forcing for all the dynamical equations, and the derivation of their estimates is given below. Note that there is no external forcing applied to the continuity equation, and thus it is not assigned a model error either, as in Jacobs and Ngodock (2003).

Consider the momentum equation (15.14) in its non-discretized form

$$\frac{\partial u}{\partial t} + \dots = \dots + \rho^{-1} F \quad (15.13)$$

where F represents the wind stress atmospheric forcing (in Nm^{-2}), the volume flux source and the tidal potential, and ρ is the water density. The model error at the surface consists of errors in the wind stress. For the subsurface, errors are assumed to arise from the volume flux and the tidal potential terms. We consider errors to be high in magnitude at the surface and decreasing with depth. Although the wind stress varies in space and time, its associated error is assumed uniform in the horizontal directions. The error magnitude is considered to be 50 % of the actual wind stress at the surface and decreasing with depth in order to mimic the decreasing impact of wind stress with depth. Two terms contribute to the forcing for the temperature equation: the net longwave, latent and sensible heat flux on one hand, and the solar radiation on the other hand. Both are assumed to be 30 % in error and the sum of their errors constitutes the forcing error in the temperature equation, with a spatial distribution similar to the one used for the errors in the momentum equation. A similar approach is taken for the errors in the salinity equation, where the forcing consists of the river inflow and evaporation minus precipitation. Forcing terms here are also considered to be 30 % in error. Finally the standard deviations for the initial condition errors are 1 m for the surface elevation, 0.5 ms^{-1} for both components of the velocity field, 2 K for temperature and 0.5PSU for salinity. These rather high errors indicate the lack of confidence in the forcing fields and initial conditions. Spatial and temporal correlation scales in (15.12) are set to 10 km and 30 h. The errors and scales above are obviously arguable, and it is not our intention to defend their choice. Rather, they are selected in this preliminary assimilation setup to demonstrate the functionality of the NCOM 4D-Var system. Smaller errors will be adopted when the system is used with real observations.

15.3.6 The Minimization

The solution of the assimilation problem is found by solving the Euler-Lagrange (EL) system of equations associated with the minimization of the cost function (15.11). The EL system is a linear yet coupled system between the adjoint and state variables. The representer methods uncouples the system by expanding the solution as the sum of a first guess and a finite linear combination of representer functions, with the representer coefficients computed by solving a linear system in

data space involving the representer matrix, the data error covariance matrix and the innovation vector. The entire representer matrix need not be computed since the linear system can be solved using an iterative algorithm (e.g. the conjugate gradient), by taking advantage of the symmetry of each matrix involved. The representer coefficients constitute the right hand side of the adjoint equation in the EL system. Once the representer coefficients are computed, they are substituted in the adjoint equation which is then solved and substituted in the forward linear equation for the final solution. A background solution around which the model is linearized is needed. Usually it is the solution of the nonlinear model. For the first guess solution, one may consider either the background or the tangent linear solution around the background. Also, the new optimal solution may replace the background for another minimization process (i.e. outer loops) until formal convergence (Bennett et al. 1996, 1998, 2002; Ngodock et al. 2000, 2007, 2009).

15.4 Experiment Setup and Results

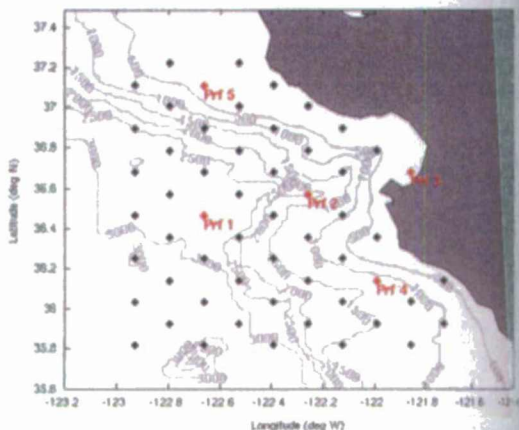
Assimilation experiments are carried out with two different data sets, and the results shown below are primarily aimed at evaluating the 4D-Var system's ability to fit both the assimilated and the non-assimilated observations.

15.4.1 MODAS Data

MODAS generates synthetic vertical profiles of temperature and salinity in the two following steps: first, a subsurface temperature is computed at a given depth using a regression from sea surface temperature and the steric component of the sea surface height anomaly. Once the subsurface temperature is computed, a corresponding subsurface salinity is computed using a climatology-based temperature/salinity relationship, Fox et al. (2002). MODAS data are thus a combination of real sea surface data (SSH and SST) and simulated sub-surface data derived from the real surface data using regression and historical relationships.

MODAS synthetics are saved and utilized in the 4D-Var analysis at intervals of 6 h. There are approximately fifty-six uniformly distributed profiles of temperature and salinity across the model domain. Each profile is represented on a vertical grid of 46 layers that do not coincide with the model's vertical grid of 41 layers, but the observation operator H in (15.10) handles the projection from the model grid to the data grid. Temperature (salinity) observation errors are set to 0.2°C (0.1 psu), and held constant through the entire assimilation window. These observation errors are purposefully set low, not because MODAS data are very accurate, but to test the assimilation's ability to reduce large discrepancies with the model, i.e. to drive the model with large errors to fit observations with small errors.

Fig. 15.2 The model domain with bathymetry contours and the profile locations, including the numbered profiles (in red) where the assimilated solution is evaluated



15.4.2 Results with MODAS Data

Starting from an initial condition on August 02, the model was integrated and the assimilation performed for 5 days at a time, with the analysis at the end of the 5 days becoming the initial condition for the following 5-day assimilation; the overall assimilation experiment interval being 30 days.

In order to assess how well the assimilation fits the observations, the analysis is examined at 5 locations in the model domain shown on Fig. 15.2. These locations are selected according to their geographic position with respect to the bay: offshore (location 1), slightly outside of the bay mouth (location 2), inside the bay (location 3), and south and north of the bay (locations 4 and 5). Results at location 2 and 4 are similar to those at location 5, and therefore are not shown.

Examining the solution in the top 500 m at the offshore location 1, it can be seen that the assimilation is able to correct large and small discrepancies between the first guess and the observations for both the temperature and salinity fields, as seen in Fig. 15.3. In the first 5 days temperature discrepancies range between 2 K in the upper 50 m, and about 1 K from 100 m and below. Likewise salinity discrepancies range from 0.15psu in the upper 200 m to 0.05psu below. These discrepancies are gradually corrected in the analysis (bottom panels of Fig. 15.3) and by the end of the first 5-day assimilation window, they have vanished. For the subsequent 5-day assimilation windows, the model temperature and salinity appear to be well constrained below 100 m with minimal to no discrepancies between the first guess and the data. Discrepancies are confined to the upper 100 m. They are small at the beginning of each 5-day window and grow with time. This is to be expected since the first guess is initialized with the previous 5-day analysis at the final time, and because the NOGAPS forcing fields are not necessarily compatible with MODAS data. That the discrepancies are confined to the upper ocean also suggests that the model error is driven by erroneous surface fluxes, although the simulation of the

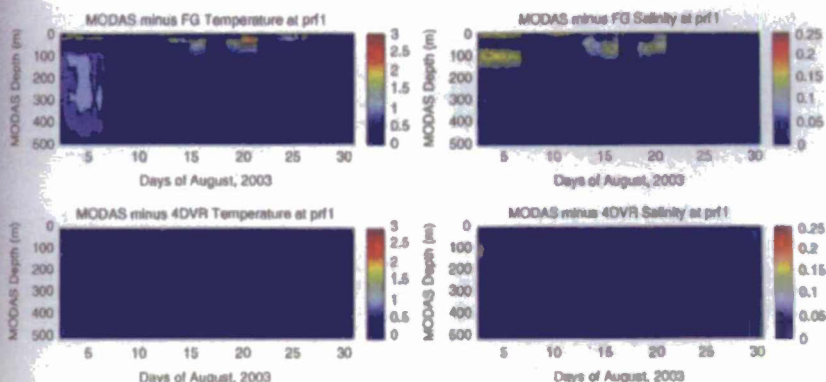


Fig. 15.3 Time evolution of the absolute value of the innovation (*top*) and the analysis error (*bottom*) at profile location 1, for temperature (*left*) and salinity (*right*)

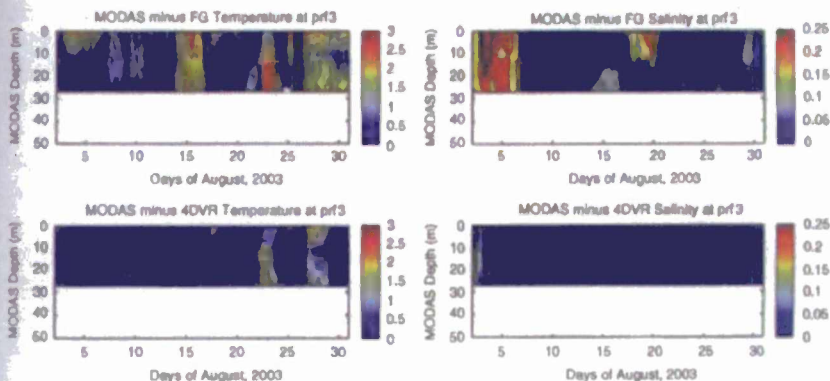


Fig. 15.4 Same as Fig. 15.3, except for location 3

mixed layer could also be incompatible with MODAS data. Yet both the data and the forcing fields are purposefully chosen in order to test the assimilation's ability to efficiently reduce these discrepancies while estimating a reasonable (magnitude-wise) correction to the surface fluxes. The assimilation effectively reduces all the discrepancies to within the data standard deviation for both temperature and salinity.

The maximum depth at location 3 inside the bay is 28 m. Results at this location, shown in Fig. 15.4, indicate that high salinity discrepancies sometimes exceeding .25psu are distributed through the water column during the first 5-day assimilation period. Some large salinity discrepancies also appear between days 18–20. Temperature discrepancies on the other hand are more prevalent, distributed over space and time. It appears that the initialization of the model using the previous 5-day analysis has less influence on the current 5-day first-guess. This may be due to the fact that in this shallow location, temporal variability of the solution is mostly governed by the

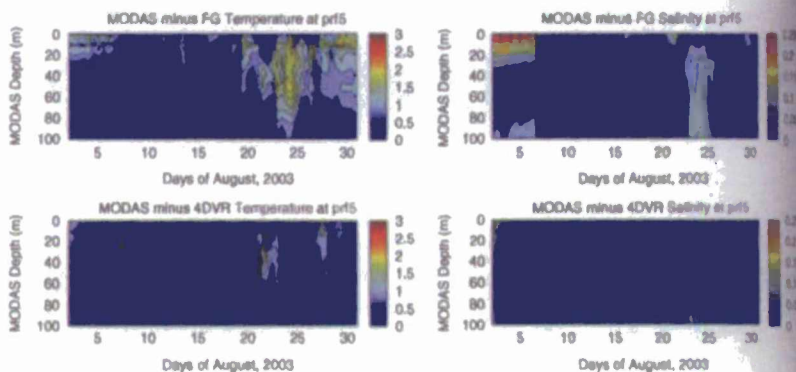


Fig. 15.5 Same as Fig. 15.3, except for location 5

local external/surface forcing coupled with strong mixing, and not by the short-lived initial conditions. Nevertheless, the assimilation still significantly reduces these discrepancies (bottom panels of Fig. 15.4) through the depth-time domain except for some isolated places. Assimilation results at location 4 (south of the mouth of the bay) are very similar to those at location 2, and therefore are not shown here.

At location 5 (north of the mouth of the bay) the maximum depth is 100 m. The largest salinity discrepancies are in the upper 20 m during the first 5-day, as seen in Fig. 15.5. There are also some moderate discrepancies in the lower layers around day 24. Temperature discrepancies are initially moderate (less than 1.5 K during the first 5-day period) and remain low until day 20, after which they start growing again, reaching 2 K. For most of the assimilation period these discrepancies are significantly reduced below 0.5 K, except for some isolated locations, e.g. around 40 m depth at days 21 and 22.

15.4.3 AOSN II Data

The dataset comprises SST from satellite and aircraft, a few SSH from satellite altimetry (due to the limited area of the model domain), vertical profiles of temperature and salinity from Slocum and Spray gliders and two moorings (M1 and M2) and AXBTs. All the vertical profiles are projected on a static grid of 42 levels.

Slocum glider tracks covered a portion of the bay, the mouth of the bay and the area to the northwest of the bay, i.e. the upwelling center around Año Nuevo. Spray glider tracks originated from the nearshore and went offshore in transect-like trajectories as seen in Fig. 15.6. To avoid redundancy some of the glider data are withheld from the assimilation and used for validation of the analyses. Withholding the data takes into account the model grid resolution and the prescribed horizontal decorrelation scale of the model error. The observations are assigned a constant error of 0.5 K and 0.3 psu in temperature and salinity respectively.

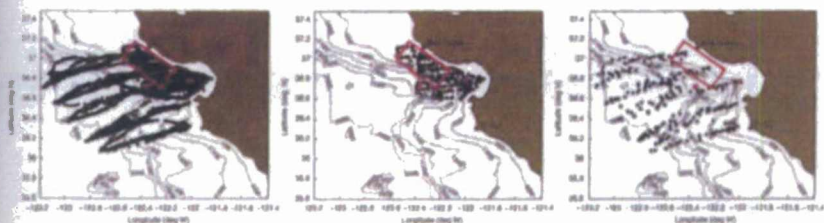


Fig. 15.6 All glider and the two mooring positions (left), and assimilated Slocum (center) and Spray (right) glider tracks during August, 2003. The red dots represent the location of the moored buoys M1 (right) and M2 (left). The red box indicates the upwelling center near Año Nuevo

15.4.4 Results with AOSN II Data

The assimilation covers the time window of August 2 to August 27, 2003, and is carried out in cycles of 5 days, with the analysis at the end of a cycle becoming the initial condition for the following cycle. Although the observations are processed and stored in 6-h intervals, the 4D-Var system assimilates all observations within the 5-day cycle simultaneously. The performance of the assimilation system is examined by computing the difference between the observations and three model solutions: (1) the free running (non assimilative) model that is integrated from the given initial conditions and forcing fields, (2) the first guess (also non assimilative) for which the initial condition is updated from the assimilation in the previous cycle, with the exception of the first cycle where both the first guess and the free running model are equal, and (3) the analysis. The first guess is also the background trajectory for the tangent linear model and the adjoint, i.e. the trajectory around which the model is linearized. It is stored in intervals of 6 h. It is anticipated that due to the re-initialization from assimilating in a previous cycle, the first guess should have smaller discrepancies with the observations than the free running model, and the analysis should have smaller discrepancies with the observations than the first guess. This should be the case for discrepancies computed with the assimilated and non-assimilated observations. It is expected of every assimilation system to fit the assimilated observations within one observation standard deviation. Unassimilated observations consist of withheld observations within the current assimilation window and future observations, those in the next cycle before the assimilation. The assimilation is expected to fit the former as a measure of the system's ability to propagate the information from the assimilated observations sites through the model space-time domain within the assimilation window. However, there is no expectation to fit future observations, i.e. the innovations in the next cycle are not expected to be smaller than the observation standard deviation. One only hopes that having initialized the model from the previous cycle's assimilation, the model forecast will remain sufficiently accurate to maintain small innovations. However, integrating the model from the initial conditions with uncorrected forcing fields is prone to drive the model away from the observations.

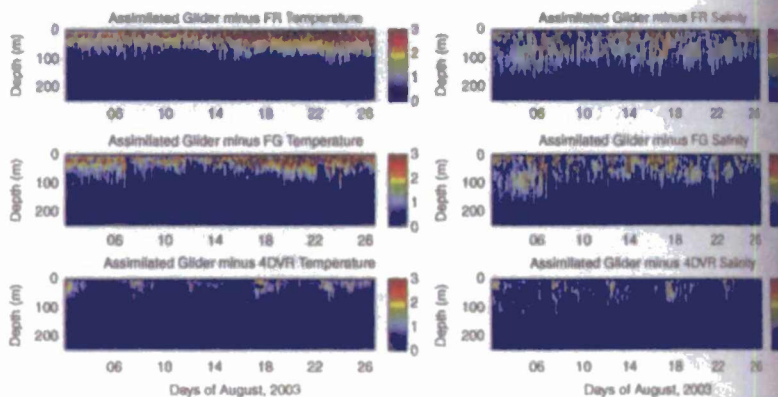


Fig. 15.7 Absolute model temperature (*left*) and salinity (*right*) discrepancies to assimilated observations for the free run (*top*), first guess (*middle*) and analysis (*bottom*)

The difference between the observations and the model is computed for all assimilated profiles of temperature and salinity and plotted in chronological order in Fig. 15.7. It can be seen that the temperature differences are confined in the upper 100 m of the water column, with magnitudes sometimes reaching 3 K for both the free run and the first guess. Salinity differences extend deeper in the water column to about 200 m, although the largest differences are confined to the upper 100 m. A slight improvement can be noticed from the free run to the forecast solutions in the temperature field, but not as much in the salinity field. However, the assimilation is able to significantly reduce the forecast discrepancies in both the temperature and salinity fields, with the exception of a few profiles at the beginning of each cycle. The assimilation is able to reduce discrepancies as high as 3 K and 0.4 psu to less than 0.5 K and 0.1 psu in temperature and salinity respectively.

The forecast solution is expected to have smaller discrepancies to the observations than the free run, because it is initialized with the analysis at the end of a previous cycle. So, having only a marginal improvement from the free run to the first guess is an indication that the gains from the assimilation are short-lived in the forecast run as a consequence of inadequate forcing fields driving the model away from future observations.

15.4.5 Independent Observations

For verification and evaluation purposes, discrepancies are computed between the withheld glider observations and the three model solutions: the free run, the first guess and the analysis. Results in Fig. 15.8 show that all three solutions have similar error levels with respect to the un-assimilated as to the assimilated observations.

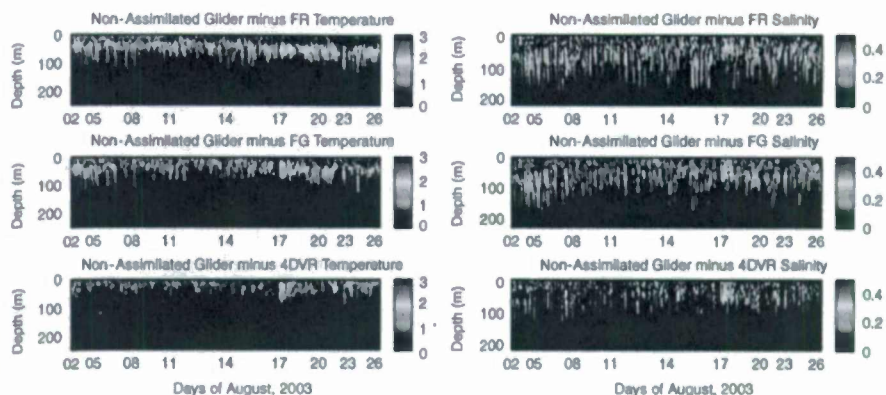


Fig. 15.8 Same as Fig. 15.7, except for non-assimilated glider observations

This result was expected because in most cases the withheld observations were located in the vicinity of assimilated observations. There are still some large temperature and salinity discrepancies in the analysis, usually around the beginning of the assimilation cycle.

15.4.6 Qualitative Fitting of the Data

The assimilation system's ability to fit the observations is further examined by comparing the differences between the observations and the free running model, the first guess and the analysis for all the observations and at all times, for both MODAS and AOSN II data. The free running model is integrated from the initial conditions and is never re-initialized, while the first guess for an assimilation cycle is initialized by the analysis at the end of the previous cycle. Elements of these difference vectors are binned by comparing their magnitude to the observations standard deviation. For example, all elements that are smaller than a standard deviation in absolute value are binned together, and so are all elements whose absolute value is between one and two standard deviations, and so on. The number of elements in each bin is then converted into a percentage of the number of assimilated observations. The results plotted as a cumulative bar chart on Fig. 15.9 show that the assimilated solution with MODAS data fits 80 % and 90 % of the observations to within one and two standard deviations respectively, while the corresponding numbers for the first guess are 60 % and 75 %, and 45 % and 63 % for the free running model. Some posterior misfits, although only a small percentage, are larger than 7 observations standard deviations, which obviously violate the Gaussian assumption on the errors in general. Similarly, for the AOSN II data, assimilated solution fits 86 % and 95 % of the observations to within one and two standard deviations respectively, while

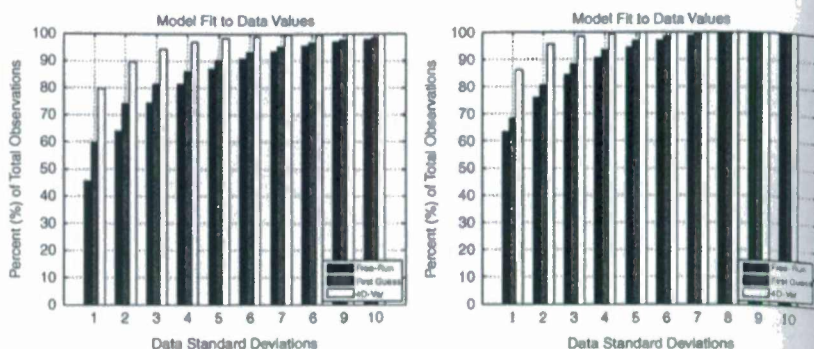


Fig. 15.9 Cumulative bar chart showing the percentage of the number of observations that are matched by the free running model (*black*), the first guess (*grey*) and the analysis (*white*) as a function of the number of observation standard deviations. MODAS experiment is shown on the left and AOSN II experiment on the right

the corresponding numbers for the first guess are 68 % and 80 %, and 64 % and 76 % for the free running model.

The large posterior misfits happened for some temperature observations with prior misfits sometimes higher than 5° , and the assimilation reduces these misfits to about 1.5° . They are larger than 7 standard deviations primarily because of very low data errors and possibly high model errors. It is assumed that a better fit would be achieved with larger observation errors and lower model errors. Such experiments (not shown here) are carried in the context of real observations and are the subject of another study.

15.5 Conclusion

A 4D-Var assimilation system for NCOM has been developed based on the indirect representer method. The system produces analysis increments for all prognostic variables (3D temperature, salinity, u- and v- components of velocity, and sea surface elevation) from a time-window of observations in a weak-constraint environment. The adjoint model has been checked against the linearized model using well established methods, verifying that the system is symmetric to within machine precision. Assimilation experiments were carried out with two different data sets.

The first experiment involved MODAS synthetic data (T , S , SSH) that were sampled every 6 h and assimilated in a sequence of 5-day time windows. Starting from an initial condition on August 02, the model was integrated and the assimilation performed for 5 days at a time, with the analysis at the end of the 5 days becoming the initial condition for the following 5-day assimilation. The results indicate that the assimilation system is performing correctly, with the model-data misfit is reduced substantially as examined at individual profiles.

The second experiment used the observations collected during AOSN II. Starting from a free run solution that completely misrepresented both the data and the dynamics of the region during the selected time period, the assimilation was able to accurately fit the assimilated data. Also, contrary to the free run and the first guess, the upwelling and relaxation events that dominate the dynamics of the regions were accurately described by the analysis which benefited from a good observation coverage of the domain and a robust assimilation system.

To avoid redundancy, some glider profiles were withheld from the assimilation and used for evaluation. The analysis fitted the withheld observations with the same accuracy as the assimilated observations. This was due in part to the proximity of the withheld observations with those that were assimilated.

The assimilated solution with MODAS data fits 80 % and 90 % of the observations to within one and two standard deviations respectively, while the corresponding numbers for the first guess are 60 % and 75 %, and 45 % and 63 % for the free running model. Some posterior misfits, although only a small percentage, are larger than 7 observations standard deviations, which obviously violate the Gaussian assumption on the errors in general. Similarly, for the AOSN II data, the assimilated solution fits 86 % and 95 % of the observations to within one and two standard deviations respectively, while the corresponding numbers for the first guess are 68 % and 80 %, and 64 % and 76 % for the free running model.

The largest discrepancies between the first guess and the observations were mostly confined to the upper ocean. After the first 5-day assimilation the first guess discrepancies grew quickly from their small initial values, confirming that the model is being forced by surface fluxes that are not compatible with the observations. This was purposefully set up in order to test the assimilation's ability to efficiently reduce these discrepancies while estimating what appears to be magnitude-wise a reasonable correction to the surface fluxes.

Acknowledgements This work was sponsored by the office of Naval Research program element number 0601153N as part of the projects "Exploring Covariances for Ocean Variational Data Assimilation" and "Variational Data Assimilation for Ocean Prediction." This paper is the Naval Research Laboratory paper contribution number JA/7320-11-646. The authors are thankful to the anonymous reviewers for their constructive remarks that helped improve the quality of this manuscript.

Appendix

The discretization of NCOM uses second-order interpolation and differentiation as defined with the notations:

$$\begin{aligned}\bar{\phi}^x &= 0.5 (\phi_{x+\Delta x/2} + \phi_{x-\Delta x/2}), \\ \left. \frac{\partial \phi}{\partial x} \right|_x &= \frac{1}{\Delta x} \delta_x \phi = \frac{1}{\Delta x} (\phi_{x+\Delta x/2} - \phi_{x-\Delta x/2}),\end{aligned}$$

and

$$\delta_{2t}\phi = (\phi_{t+\Delta t} - \phi_{t-\Delta t})$$

The NCOM equations are then discretized in flux conservative form as follows

$$\begin{aligned} \frac{\Delta x^u \Delta y^u}{2\Delta t} \delta_{2t}(\Delta z^u u) &= \overline{\Delta x \Delta y \Delta z (f + C_{curv})} \bar{v}^y{}^x - \Delta y^u \Delta z^u g \delta_x (\zeta^* + \zeta_{atm} - \zeta_{tp}) \\ &\quad - \Delta x^u \Delta z^u \frac{1}{\rho_0} \delta_x (p_i) \\ &\quad - \delta_x \left(\overline{\Delta y^u \Delta z^u u^a{}^x} \bar{u}^x \right) - \delta_y \left(\overline{\Delta x^u \Delta z^u v^a{}^x} \bar{u}^y \right) \\ &\quad - \delta_z \left(\overline{\Delta x \Delta y w^x} \bar{u}^z \right) \\ &\quad + \overline{\Delta x \Delta y \Delta z Q^x} u_{sor} + F_u^* \\ &\quad + \Delta x^u \Delta y^u \delta_z \left(\frac{\bar{K}_M^x}{(\bar{\Delta z}^w{}^x)^{n+1}} \delta_z u^{n+1} \right) \end{aligned} \quad (15.14)$$

$$\begin{aligned} \frac{\Delta x^v \Delta y^v}{2\Delta t} \delta_{2t}(\Delta z^v v) &= \overline{\Delta x \Delta y \Delta z (f + C_{curv})} \bar{u}^x{}^y - \Delta x^v \Delta z^v g \delta_y (\zeta^* + \zeta_{atm} - \zeta_{tp}) \\ &\quad - \Delta x^v \Delta z^v \frac{1}{\rho_0} \delta_y (p_i) \\ &\quad - \delta_x \left(\overline{\Delta y^v \Delta z^v u^a{}^y} \bar{v}^x \right) - \delta_y \left(\overline{\Delta x^v \Delta z^v v^a{}^x} \bar{v}^y \right) \\ &\quad - \delta_z \left(\overline{\Delta x \Delta y w^y} \bar{v}^z \right) \\ &\quad + \overline{\Delta x \Delta y \Delta z Q^y} v_{sor} + F_v^* \\ &\quad + \Delta x^v \Delta y^v \delta_z \left(\frac{\bar{K}_M^y}{(\bar{\Delta z}^w{}^y)^{n+1}} \delta_z v^{n+1} \right) \end{aligned} \quad (15.15)$$

$$\frac{\Delta x \Delta y}{2\Delta t} \delta_{2t}(\Delta z) = -\delta_x (\Delta y^u \Delta z^u u^a) - \delta_y (\Delta x^v \Delta z^v v^a) - \delta_z (\Delta x \Delta y w) \quad (15.16)$$

$$\begin{aligned} \frac{\Delta x \Delta y}{2\Delta t} \delta_{2t}(\Delta z T) &= -\delta_x (\Delta y^u \Delta z^u u^a \bar{T}^x) - \delta_y (\Delta x^v \Delta z^v v^a \bar{T}^y) \\ &\quad - \delta_z (\Delta x \Delta y w \bar{T}^z) \\ &\quad + \Delta x \Delta y \Delta z Q T_{sor} + \delta_x \left(\frac{\Delta y^u \Delta z^u A_H^u}{\Delta x^u} \delta_x T^{n-1} \right) \end{aligned}$$

$$\begin{aligned}
& + \delta_y \left(\frac{\Delta y^v \Delta z^v A_H^v}{\Delta y^v} \delta_y T^{n-1} \right) \\
& + \Delta x \Delta y \delta_z \left(\frac{K_H}{(\Delta z^w)^{n+1}} \delta_z T^{n+1} \right) + \Delta x \Delta y Q_r \delta_z \gamma \quad (15.17)
\end{aligned}$$

$$\begin{aligned}
\frac{\Delta x \Delta y}{2 \Delta t} \delta_{2t} (\Delta z S) & = -\delta_x (\Delta y^u \Delta z^u u^u \bar{S}^x) - \delta_y (\Delta x^v \Delta z^v v^v \bar{S}^y) - \delta_z (\Delta x \Delta y w \bar{S}^z) \\
& + \Delta x \Delta y \Delta z Q S_{sor} + \delta_x \left(\frac{\Delta y^u \Delta z^u A_H^u}{\Delta x^u} \delta_x S^{n-1} \right) \\
& + \delta_y \left(\frac{\Delta y^v \Delta z^v A_H^v}{\Delta y^v} \delta_y S^{n-1} \right) \\
& + \Delta x \Delta y \delta_z \left(\frac{K_H}{(\Delta z^w)^{n+1}} \delta_z S^{n+1} \right) \quad (15.18)
\end{aligned}$$

In (15.14, 15.15, 15.16, 15.17 and 15.18), F_u and F_v are the horizontal mixing terms, ζ_{atm} and ζ_{tp} are the atmospheric surface pressure and tidal potential respectively, and ζ^* is the surface elevation term that can be distributed among any of the three time levels, $\zeta^* = \alpha_1 \zeta^{n+1} + \alpha_2 \zeta^n + \alpha_3 \zeta^{n-1}$, according to the temporal weighting terms α_1 , α_2 , or α_3 , which are specified by the user. A_M and A_H are the horizontal mixing coefficients for the velocity and scalar fields (temperature and salinity) respectively, likewise K_M and K_H for the vertical mixing, Q is a volume flux source term (with T_{sor} , S_{sor} , u_{sor} , and v_{sor} as the term source values), Q_r is the solar radiation, γ is a function describing the solar extinction, Δx , Δy and Δz denote the grid-cell dimensions defined at the center of the grid cells, and the superscripts u , v and w indicate the grid-cell dimensions computed at those velocity locations on the staggered Arakawa C-grid. f is the Coriolis term, ρ_0 and p_i are the reference density of seawater and the internal pressure, respectively, and the horizontal advection velocity terms are given by u^a and v^a . The term C_{curv} is used to correct the horizontal advection of momentum for the horizontal curvature of the grid. It is calculated as

$$C_{curv} = \bar{v}^y \frac{\delta_{2x}(\Delta y)}{2 \Delta x \Delta y} - \bar{u}^x \frac{\delta_{2y}(\Delta x)}{2 \Delta x \Delta y} \quad (15.19)$$

The horizontal mixing terms for the momentum equations are given by

$$\begin{aligned}
F_u^* & = \delta_x \left(2 \left(\frac{\Delta y^u \Delta z^u A_M^u}{\Delta x^u} \right)^x \delta_x u^{n-1} \right) \\
& + \delta_y \left(\left(\frac{\Delta x^v \Delta z^v A_M^v}{\Delta y^v} \right)^x \delta_y u^{n-1} + \left(\frac{\Delta x^v \Delta z^v A_M^v}{\Delta x^v} \right)^x \delta_x v^{n-1} \right) \quad (15.20)
\end{aligned}$$

$$F_v^* = \delta_x \left(\left(\frac{\Delta y^u \Delta z^u A_M^u}{\Delta y^u} \right)^y \delta_y u^{n-1} + \left(\frac{\Delta y^u \Delta z^u A_M^u}{\Delta x^u} \right)^y \delta_x v^{n-1} \right) + \delta_y \left(2 \left(\frac{\Delta x^v \Delta z^v A_M^v}{\Delta y^v} \right)^y \delta_y v^{n-1} \right) \quad (15.21)$$

where the mixing coefficient is modeled according to the Smagorinsky formula

$$A_M = C_{Smag} \Delta x \Delta y \left[\left(\frac{1}{\Delta x} \delta_x u^n \right)^2 + \frac{1}{2} \left(\frac{1}{2\Delta y} \delta_{2y} \overline{u^n} + \frac{1}{2\Delta x} \delta_{2x} \overline{v^n} \right)^2 + \left(\frac{1}{\Delta y} \delta_y v^n \right)^2 \right]^{\frac{1}{2}} \quad (15.22)$$

with the magnitude of the eddy coefficient being scaled by the constant C_{smag} . The vertical mixing coefficients are computed using the turbulence closure by Mellor and Yamada in either 2 or 2.5 version.

The computation for the free-surface mode is governed by the equations:

$$\frac{\Delta x^u \Delta y^u}{2\Delta t} \delta_{2t} (D^u \bar{u}) = -\Delta y^u D^u g \delta_x (\alpha_1 \zeta^{n+1} + \alpha_2 \zeta^n + \alpha_3 \zeta^{n-1}) + D^u \overline{G_u} \quad (15.23)$$

$$\frac{\Delta x^v \Delta y^v}{2\Delta t} \delta_{2t} (D^v \bar{v}) = -\Delta x^v D^v g \delta_y (\alpha_1 \zeta^{n+1} + \alpha_2 \zeta^n + \alpha_3 \zeta^{n-1}) + D^v \overline{G_v} \quad (15.24)$$

$$\begin{aligned} \frac{\Delta x \Delta y}{2\Delta t} \delta_{2t} \zeta = & -\delta_x \left(\Delta y^u \left(\beta_1 (\overline{D^u u})^{n+1} + \beta_2 (\overline{D^u u})^n + \beta_3 (\overline{D^u u})^{n-1} \right) \right) \\ & -\delta_y \left(\Delta x^v \left(\beta_1 (\overline{D^v v})^{n+1} + \beta_2 (\overline{D^v v})^n + \beta_3 (\overline{D^v v})^{n-1} \right) \right) \\ & + \Delta x \Delta y D \overline{Q}, \end{aligned} \quad (15.25)$$

where β_1, β_2 and β_3 are positive constants define by the user with $\beta_1 + \beta_2 + \beta_3 = 1$. $D^u \overline{G_u}$ and $D^v \overline{G_v}$ are the vertical integrals of all the terms in the right hand side of (15.14) and (15.15) respectively, with the exception of the surface elevation gradient terms and the vertical mixing, and $D^u = \bar{D}^x$ and $D^v = \bar{D}^y$. The free-surface mode (15.25) is solved by first substituting $(D^u \bar{u})^{n+1}$ and $(D^v \bar{v})^{n+1}$ from the time discretized (15.23) and (15.24) into (15.25), resulting in an elliptic equation that is solved for the surface elevation at time level $n + 1$, which is then substituted back in (15.23) and (15.24) for computing the barotropic transports $D^u \bar{u}$ and $D^v \bar{v}$ from which the barotropic velocities are obtained.

The vertical discretization uses a combination of sigma layers and z-levels in a three-tiered distribution with (1) free sigma layers near the surface that expand and contract with the free surface elevation, (2) fixed sigma layers that do not vary with the free surface, and (3) fixed z levels that allow for partial bottom cells for a better match of the bottom topography.

References

- Amodei L (1995) Solution approchée pour un problème d'assimilation de données avec prise en compte de l'erreur du modèle. *Comptes Rendus de l'Académie des Sciences* 321:Série IIa, 1087–1094
- Barron CN, Kara AB, Martin PJ, Rhodes RC, Smedstad LF (2006) Formulation, implementation and examination of vertical coordinate choices in the Global Navy Coastal Ocean Model (NCOM). *Ocean Model* 11:347–375
- Bennett AF (1992) *Inverse methods in physical oceanography*. Cambridge University Press, New York, 347 pp
- Bennett AF (2002) *Inverse modeling of the ocean and atmosphere*. Cambridge University Press, Cambridge, UK/NY
- Bennett AF, Chua BS, Leslie LM (1996) Generalized inversion of a global numerical weather prediction model. *Meteorol Atmos Phys* 60:165–178
- Bennett AF, Chua BS, Harrison ED, McPhaden MJ (1998) Generalized inversion of Tropical Atmosphere-Ocean (TAO) data and a coupled model of the tropical Pacific. *J Climate* 11:1768–1792
- Bischof C, Corliss G, Green L, Griewank A, Haigler K, Newman P (1992) Automatic differentiation of advanced CFD codes for multidisciplinary design. *Comput Syst Eng* 3(6):625–637
- Broquet G, Edwards CA, Moore AM, Powell BS, Veneziani M, Doyle JD (2009) Application of 4D-variational data assimilation to the California Current System. *Dyn Atmos Oceans* 48:69–92
- Broquet G, Moore AM, Arango HG, Edwards CA (2011) Corrections to ocean surface forcing in the California Current System using 4D variational data assimilation. *Ocean Model* 36:116–132
- Chao Y, Li ZJ, Farrara J, McWilliams JC, Bellingham J, Capet X, Chavez F, Choi JK, Davis R, Doyle J, Fratantoni DM, Li P, Marchesiello P, Moline MA, Paduan J, Ramp S (2009) Development, implementation and evaluation of a data-assimilative ocean forecasting system off the central California coast. *Deep-Sea Res Part II-Top Stud Oceanogr* 56(3–5):100–126
- Chua BS, Bennett AF (2001) An inverse ocean modeling system. *Ocean Model* 3:137–165
- Daley R (1992) *Atmospheric data analysis*. Cambridge University Press, Cambridge, NY, 472 pp
- Daley R, Barker E (2001) NAVDAS formulation and diagnostics. *Mon Weather Rev* 129:869–883
- Derber J, Rosati A (1989) A global oceanic data assimilation system. *J Phys Oceanogr* 19:1333–1347
- Di Lorenzo E, Moore A, Arango H, Chua, B, Cornuelle BD, Miller AJ, Powell B, Bennett A (2007) Weak and strong constraint data assimilation in the inverse Regional Ocean Modeling System (ROMS): development and application for a baroclinic coastal upwelling system. *Ocean Model* 16(3–4):160–187
- Egbert GD, Bennett AF, Foreman MGG (1994) TOPEX/POSEIDON tides estimated using a global inverse method. *J Geophys Res* 99:24821–24852
- Erwig M, Fu Z, Pflaum B (2007) Parametric fortran: program generation in scientific computing. *J Software Mainten Evol* 19(3):155–182
- Fox DN, Teague WJ, Barron CN, Carnes MR, Lee CM (2002) The modular ocean data assimilation system (MODAS). *J Atmos Ocean Technol* 19:240–252
- Giering R, Kaminski T (1998) Recipes for adjoint code construction. *ACM Trans Math Software* 24(4):437–474
- Goerss JS, Phoebus PA (1992) The Navy's operational atmospheric analysis. *Weather Forecast* 7:232–249
- Haley PJ, Lermusiaux PFJ, Robinson AR, Leslie WG, Logoutov O, Cossarini G, Liang XS, Moreno P, Ramp SR, Doyle JD, Bellingham J, Chavez F, Johnston S (2009) Forecasting and reanalysis in the Monterey Bay/California current region for the autonomous ocean sampling network-II experiment. *Deep-Sea Res Part II-Top Stud Oceanogr* 56(3–5):127–148
- Hascoet L, Pascual V (2004) Tapenade 2.1 user's guide. Rapport INRIA n 300, 2004; 78. Available from <http://www.inria.fr/rrrt/rt-0300.html>

- Hodur Richard M (1997) The naval research laboratory's coupled ocean/atmosphere mesoscale prediction system (COAMPS). *Mon Weather Rev* 125:1414–1430
- Jacobs GA, Ngodock HE (2003) The maintenance of conservative physical laws within data assimilation systems. *Mon Weather Rev* 131:2595–2607
- Marotzke J, Giering R, Zhang KQ, Stammer D, Hill C, Lee T (1999) Construction of the adjoint MIT ocean general circulation model and application to Atlantic heat transport sensitivity. *J Geophys Res* 104(C12):29, 529–29, 547
- Martin P (2000) Description of the navy coastal ocean model version 1.0. NRL report NRL/FR/7322—00–9961
- Moore AM, Arango HG, Di Lorenzo E, Cornuelle BD, Miller AJ, Neilson DJ (2004) A comprehensive ocean prediction and analysis system based on the tangent linear and adjoint of a regional ocean model. *Ocean Model* 7:227–258
- Ngodock HE (2005) Efficient implementation of covariance multiplication for data assimilation with the representer method. *Ocean Model* 8(3):237–251
- Ngodock HE, Chua BS, Bennett AF (2000) Generalized inversion of a reduced gravity primitive equation ocean model and tropical atmosphere ocean data. *Mon Weather Rev* 128:1757–1777
- Ngodock HE, Jacobs GA, Chen M (2006) The representer method, the ensemble Kalman filter and the ensemble Kalman smoother: a comparison study using a nonlinear reduced gravity ocean model. *Ocean Model* 12:378–400
- Ngodock HE, Smith SR, Jacobs GA (2007) Cycling the representer algorithm for variational data assimilation with the Lorenz attractor. *Mon Weather Rev* 135:373–386
- Ngodock HE, Smith SR, Jacobs GA (2009) Cycling the representer method with nonlinear models. In: *Data assimilation for atmospheric, oceanic & hydrologic applications*. Springer, Berlin
- Peyton Jones SL (2003) Haskell 98 language and libraries: the revised report. Cambridge University Press, Cambridge, UK, 270 pp
- Rosenfeld LK, Schwing FB, Garfield N, Tracy DE (1994) Bifurcated flow from an upwelling center: a cold water source for Monterey Bay. *Continental Shelf Res* 14:931–964
- Rosmond TE (1992) The design and testing of the Navy Operational Global Atmospheric Prediction System. *Weather Forecast* 7:262–262
- Shulman I, Wu CR, Lewis JK, Paduan JD, Rosenfeld LK, Kindle JC, Ramp SR, Collins CA (2002) High resolution modeling and data assimilation in The Monterey Bay. *Continental Shelf Res* 22(8):1129–1151
- Shulman I, Rowley C, Anderson S, DeRada S, Kindle J, Martin P, Doyle J, Cummings J, Ramp S, Chavez F, Frantoni D, Davis R (2009) Impact of glider data assimilation on the Monterey Bay Model. *Deep Sea Res* 56:188–198
- Smith SR, Ngodock HE (2008) Cycling the representer algorithm for 4D-variational data assimilation with the Navy Coastal Ocean Model. *Ocean Model* 24:92–107
- Stammer D, Wunsch C, Giering R, Eckert C, Heimbach P, Marotzke J, Adcroft A, Hill CN, Marshall J (2002) The global ocean circulation during 1992–1997, estimated from ocean observations and a general circulation model. *J Geophys Res* 107:C9 3118
- Talagrand O (1999) A posteriori evaluation and verification of analysis and assimilation algorithms. In: *Proceedings of workshop on diagnosis of data assimilation system held at ECMWF, Shinfield Park*, pp 17–28
- Weaver A, Courtier P (2001) Correlation modeling on the sphere using a generalized diffusion equation. *Q J Roy Meteorol Soc* 127:1815–1846
- Weaver AT, Vialard J, Anderson DLT (2003) Three- and four-dimensional variational assimilation with a general circulation model of the tropical Pacific Ocean. Part I: formulation, internal diagnostics, and consistency checks. *Mon Weather Rev* 131(7):1360–1378
- Wunsch C (2006) Discrete inverse and state estimation problems. With geophysical fluid applications. Cambridge University Press, Cambridge, 371 pp